Research Article | Vol. 29, No. 17 / 16 August 2021 / Optics Express 26831
Optics EXPRESS

Optical feedback linear cavity enhanced absorption spectroscopy

JIANFEI TIAN,[1,2] GANG ZHAO,[1,2,4] ADAM J. FLEISHER,[3] WEIGUANG MA,[1,2,5] AND SUOTANG JIA[1,2]

[1]State Key Laboratory of Quantum Optics & Quantum Optics Devices, Institute of Laser Spectroscopy, Shanxi University, 030006 Taiyuan, China
[2]Collaborative Innovation Center of Extreme Optics, Shanxi University, 030006 Taiyuan, China
[3]Material Measurement Laboratory, National Institute of Standards and Technology, 100 Bureau Drive, Gaithersburg, MD 20899, USA
[4]gangzhao@sxu.edu.cn
[5]mwg@sxu.edu.cn

Abstract: A simple and universal technique for performing optical feedback cavity enhanced absorption spectroscopy with a linear Fabry-Pérot cavity is presented. We demonstrate through both theoretical analysis and experiment that a diode laser can be sequentially stabilized to a series of cavity modes without any influence from the direct reflection if the feedback phase is appropriately controlled. With robust handling of the feedback phase and help from balanced detection, a detection limit of 1.3×10^{-9} cm^{-1} was achieved in an integration time of 30 s. The spectrometer performance enabled precision monitoring of atmospheric methane (CH_4) concentrations over a time period of 72 h.

1. Introduction

Cavity enhanced spectroscopy is an excellent candidate for trace gas detection due to its high sensitivity. The technique benefits from an extension of the interaction path length between light and the targeted gas, which is proportional to the cavity finesse [1,2]. Advancements in coating technologies, such as physical vapor deposition and substrate-transferred crystalline coatings, have enabled fabrication of high performance cavity mirrors with total mirror losses down to 10^{-6} [3,4]. The result is optical cavities with finesse up to 5×10^5 and equivalent absorption path length up to hundreds of km [5].

Cavity enhanced absorption spectroscopy (CEAS) is one of the basic types of cavity enhanced spectroscopy. It directly measures cavity transmission to deduce intracavity absorption by attenuation. When afflicted by inferior coupling efficiency induced by frequency mismatch between the laser and the cavity mode, cavity transmission can fluctuate to a large extent from mode to mode, consequently degrading detection sensitivity [6]. This effect is especially evident when coupling diode lasers with broad linewidths (larger frequency noise) to high finesse cavities with a narrow mode width. To mitigate the effects of frequency mismatch, different methodologies have been proposed. The most common one is cavity ring-down spectroscopy (CRDS) [7]. With the incident light off, CRDS leverages the shortening of the intracavity power decay time constant in order to measure intracavity absorption and thus is immune to variations of the initial cavity transmission that arise from both laser residual intensity noise and any instability of the coupling efficiency. Integrated cavity output spectroscopy (ICOS), often used in a type of off-axis ICOS (OA-ICOS), measures dozens of cavity transverse modes simultaneously to average over their coupling efficiencies. However, the drawback is a significantly reduced cavity enhancement factor and therefore limited performance [8].

Optical feedback CEAS (OF-CEAS) can directly address mode-to-mode variations in transmission intensity by greatly improving the laser-cavity coupling [9]. The leak-out from the intracavity

#431934 https://doi.org/10.1364/OE.431934
Journal © 2021 Received 24 May 2021; revised 19 Jul 2021; accepted 27 Jul 2021; published 4 Aug 2021

Optics EXPRESS

light is directed back to laser to establish self-stabilization of the laser frequency to the resonant frequency of a cavity mode. Ideally, this will result in all of the laser power being coupled into the cavity and stable cavity transmission should be observed. The advantages of OF-CEAS have been widely demonstrated with different types of diode lasers [10–13]. Following the first implementation in 2005 by Morville et al., most OF-CEAS setups are based on a V-shaped cavity geometry [14]. The V-shaped cavity geometry can readily separate intracavity leak-out from unwanted direct reflection at the cavity front mirror. Consequently, only the former optical field can induce optical feedback self-locking. However, compared with a linear Fabry-Pérot cavity (the most common cavity used in CEAS), V-shape cavities possess lower finesse due to additional loss from the third cavity mirror and are more sensitive to vibration noise.

Previous efforts towards OF-CEAS with linear cavities required uncommon experimental methods. There, in order to spatially filter the direct reflection to avoid competition between optical feedback from intracavity leak-out and direct reflection fields, the deliberate introduction of mode mismatching followed by an iris was reported. Also, the redirection of the cavity transmission rather than cavity reflection back to laser has been reported. Those extra measures added complexity to each system and degraded universality [15–17]. Our recent work has shown that a mid-infrared quantum-cascade laser (QCL) could be stabilized to one cavity longitudinal mode via optical feedback, and that a narrow laser linewidth down to the Hz level could be achieved for short times [18,19]. Enabled by high intracavity powers and tight coupling, the narrow linewidth QCL operating at a wavelength of 4.5 μm was used to perform two-photon cavity ring-down spectroscopy for the first time.

In this paper, a simple and universal OF-CEAS based on a linear cavity is presented. Initially, an expression for the laser frequency with optical feedback is provided. It shows that the direct reflection does not compete with the desired optical feedback from the cavity leak-out field if the feedback phase is carefully controlled. Then, a cavity enhanced absorption signal is obtained using the self-stabilization technique with a near-infrared (NIR) distributed feedback (DFB) diode laser. Finally, we evaluate the detection limit of the optical system and apply the instrument to monitor methane (CH_4) concentrations in the air with high precision.

2. Theory

Figure 1 shows a schematic illustration of optical feedback from a linear cavity to a diode laser. The laser gain medium has a length of L_d and electric field reflection coefficients of r_b and r_0 for back and output facets, respectively. The Fabry-Pérot cavity with length of L_c consists of two similar mirrors with field reflectivity coefficients of r_m. The triangle symbol represents loss during the path between laser and cavity with round-trip power attenuation of β, and the length between the laser output facet and cavity front mirror is L_a. In this section, we assume that β is the same for all light returning to the laser. The leak-out of intracavity light from the front mirror of the cavity is referred to as resonant reflection light and direct reflection from the cavity front mirror is referred to as non-resonant reflection light.

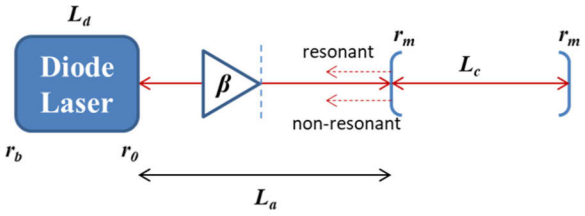

Fig. 1. Schematic illustration of optical feedback from a linear cavity to a diode laser.

Optics EXPRESS

In the case of weak feedback, where $\beta << 1$, the rate equations that describes the evolution of the electric field amplitude versus time (t) at the laser output facet can be written as

$$\begin{aligned}\frac{d}{dt}[E(t)e^{i(\omega t+\phi(t))}] = &\left[i\omega_{\text{free}} + \frac{1}{2}(G-\Gamma)(1+i\alpha)\right]E(t)e^{i(\omega t+\phi(t))} + \\ &K\tilde{h}_{\text{r}}^{(\text{res})}E(t-\tau_{\text{a}})e^{i[\omega(t-\tau_{\text{a}})+\phi(t-\tau_{\text{a}})]} + \\ &K\tilde{h}_{\text{r}}^{(\text{non res})}E(t-\tau_{\text{a}})e^{i[\omega(t-\tau_{\text{a}})+\phi(t-\tau_{\text{a}})]},\end{aligned} \tag{1}$$

where ω is the coupled laser angular frequency, ϕ is the phase shift due to time-dependent fluctuations in the laser electric field, ω_{free} is the free-running laser angular frequency without optical feedback, G is the net rate of stimulated emission, Γ is the photon decay rate, and α is Henry-Factor [20]. The second and third items on the right side of Eq. (1) are introduced by optical feedback from resonant and non-resonant light, respectively. The roundtrip delay time between the laser and the cavity front mirror, τ_{a}, is equal to $2L_{\text{a}}/c$, where c is the speed of light. The empty-cavity steady-state reflection transfer functions for resonant, $\tilde{h}_{\text{r}}^{(\text{res})}$, and non-resonant light, $\tilde{h}_{\text{r}}^{(\text{non res})}$, at the laser output facet are defined in Eqs. (2)–(3) as

$$\tilde{h}_{r}^{(\text{res})} = \frac{t_{\text{m}}^2}{r_{\text{m}}}\frac{r_{\text{m}}^2 e^{-i\omega\tau_{\text{c}}}}{1-r_{\text{m}}^2 e^{-i\omega\tau_{\text{c}}}} \quad \text{and} \tag{2}$$

$$\tilde{h}_{\text{r}}^{(\text{non res})} = -r_{\text{m}}, \tag{3}$$

where τ_{c} represents the round-trip time of the laser within the external linear cavity, equal to $2L_{\text{c}}/c$ [21,22]. In Eq. (2)–(3), t_{m} is the external cavity mirror electric field transmission coefficient. The minus sign in Eq. (3) properly defines the relative phase of the non-resonant light to be one half-cycle out of phase with the resonant leak-out light. The feedback coupling rate pre-factor, K, in Eq. (1) is written as

$$K = \sqrt{1+\alpha^2}\frac{c}{2nL_{\text{d}}}\sqrt{\beta}\frac{1-r_0^2}{r_0}, \tag{4}$$

where $c/(2nL_{\text{d}})$ is the free spectral range of the diode laser with gain medium refractive index n.

For a steady-state condition of the laser, we substitute $dE/dt = 0$ and $d\phi/dt = 0$ into Eq. (1). Then the coupled laser frequency, i.e. ω, is given by

$$\omega_{\text{free}} = \omega + K_1\frac{\sin[\omega(\tau_{\text{a}}+\tau_{\text{c}})+\theta] - r_{\text{m}}^2\sin[\omega\tau_{\text{c}}+\theta]}{1+F^2\sin^2(\omega\tau_{\text{c}}/2)} - K_2\sin(\omega\tau_{\text{a}}+\theta), \tag{5}$$

where $K_1 = Kr_{\text{m}}/(1-r_{\text{m}}^2)$, $K_2 = Kr_{\text{m}}$, $F = 2r_{\text{m}}/(1-r_{\text{m}}^2)$ and $\theta = \arctan(\alpha)$. The second and third terms arise from optical feedback from resonant and non-resonant light, respectively. When there is no optical feedback, $K_1 = 0$ and $K_2 = 0$, and therefore $\omega_{\text{free}} = \omega$.

A simulation of the coupled laser frequency calculated using Eq. (5) is shown in Fig. 2. The right panel is a zoom-in of the central part. In the simulation, we assume $r_{\text{m}}^2 = 0.99986$, $L_c = 39.4$ cm, $\beta = 3\times10^{-5}$, $\alpha = 2$, $L_{\text{d}} = 0.1$ cm, $n = 3.5$ and $r_0 = 0.6$. Both the x- and y-axes show the laser frequency detuning relative to the q_{th} cavity longitudinal mode of frequency ν_q and angular frequency $\omega_q = 2\pi\nu_q$, chosen so that $\omega_q\tau_{\text{c}}$ is equal to $2q\pi$. To maximize optical feedback from resonant light, L_{a} is set to be close to an integer multiple of L_{c} in order to meet the general coupling condition that $\omega_q\tau_{\text{a}} + \theta$ is equal to $2m\pi$ where, like q, m is also an integer.

The black dashed-dotted line in Fig. 2 represents the laser frequency without optical feedback, when only the first term in Eq. (5) contributes to the linear response. The blue curve is the result with optical feedback only from non-resonant light, so another component, i.e. the third item in the right of Eq. (5), is included. As a result, an additional modulation is superposed on the

Optics EXPRESS

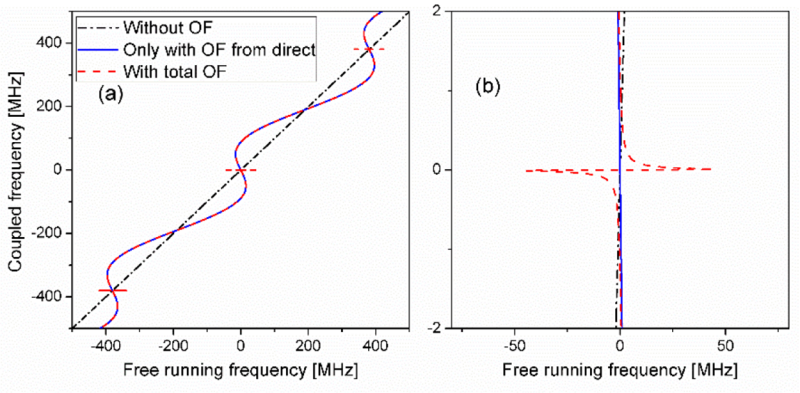

Fig. 2. Simulation of the coupled laser frequency versus the free-running laser frequency. For the simulation, $L_a \approx L_c$.

simulated laser frequency. When the coupled laser frequency is close to the cavity mode, the blue curve approaches the black dashed line, indicating that the influence of optical feedback from the non-resonant light vanishes at the cavity mode. The red dashed curve is based on the complete model with consideration of optical feedback from both non-resonant and resonant light. When the free-running laser frequency is far away from a cavity longitudinal mode, there is no light leaking out from the cavity, and therefore the red dashed curve coincides with the blue. When it is close to the cavity mode, the leak-out from the cavity causes the strong distortion in the red dashed curve and the coupled laser frequency is stabilized to the cavity longitudinal mode frequency, illustrated by the flat platform. This model is consistent with the physical insight that when the relative phase of the resonant light is a multiple of 2π, i.e. in-phase with light in the laser gain medium, optical feedback from the leak-out field will force the laser frequency to be stabilized to the external linear cavity. The non-resonant light is out-of-phase with the laser light at the cavity mode frequency and thus will have minimal influence on optical feedback and the locking range, i.e. the width of the platform, dependent on β, could be 100s of MHz.

The model presented above assumes steady-state laser operation and external cavity pumping. Up to this point, it does not include perturbations due to the preferential clipping of one of the two reflected fields on its return path to the laser, spatial interference effects, model asymmetries near cavity resonance due to slight deviations in the laser-cavity path length, mirror birefringence, or laser dynamics and coupled-cavity transient events. Each one of these phenomena could potentially reduce model accuracy when compared to experiment.

3. Experiment

The experimental setup for optical feedback linear cavity enhanced absorption spectroscopy (OF-LCEAS) is shown in Fig. 3. The light source is a DFB laser (Eblana, TTP190719247) with output power of 6.5 mW and TO footprint mounted on a translation stage [23]. The laser light, emitted at a wavelength of 1.65 μm and addressing three overlapping CH_4 transition at 6046.9 cm^{-1}, passes through several reflecting mirrors, a half wave plate, a polarization beam splitter (PBS) cube, quarter wave plate, mode-matching lens and then impinges onto the linear cavity. The linear cavity is Fabry-Pérot type and consists of two planoconcave mirrors with 1-m radius of curvature. The two mirrors have reflectivity of 99.92%, corresponding to a finesse of 3900 and cavity mode width of 100 kHz. The mirrors are separated by an invar steel tube with length of 39.4 cm, resulting in a free spectral range of 380 MHz. The distance between the laser output facet and cavity front mirror, adjusted coarsely by the laser precision translation stage and finely

Optics EXPRESS

by a piezoelectric transducer (PZT) adhered to one of the steering mirrors, is set to almost two times the cavity length ($L_a \approx 2L_c$). The cavity transmission is recorded by a detector (Thorlabs PDA 10CS-EC).

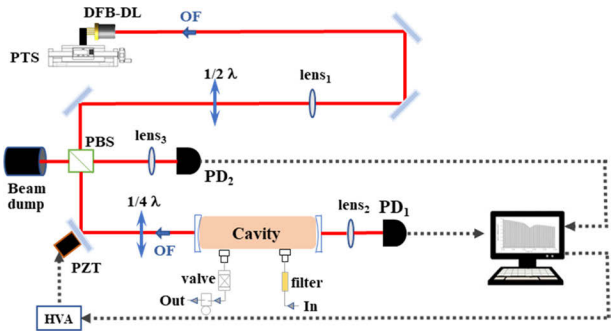

Fig. 3. Experimental setup for optical feedback linear cavity enhanced absorption spectroscopy, OF-LCEAS. DFB-DL: distributed feedback diode laser; PTS: precision translation stage; 1/2 λ: half wave plate; 1/4 λ: quarter wave plate; PBS: polarization beam splitter; PZT: piezoelectric transducer; HVA: high voltage amplifier; $PD_{1,2}$: photodetectors.

To monitor the variation of laser output power during OF-LCEAS, part of light was separated by the PBS and sent to photodetector number 2 (PD_2). Then, the signal from PD_2 was subtracted from the cavity transmission signal at the output of PD_1, achieving balanced detection. The amount of light sent to PD_2 was controlled by the half wave plate shown in Fig. 3. The feedback ratio for the power returning to the laser could be adjusted by rotating a quarter wave plate without sacrificing any of the power incident on the linear cavity, and the reflected light rejected by the PBS was sent to a beam dump. By precision measurement of the incident, off- and on-resonant reflected, and transmitted laser powers [24,25], we report a mode-matched power coupling fraction for our OF-LCEAS system of 0.37, resulting in an intracavity power of 2.3 W at an incident power of 2 mW. For spectroscopy, the laser frequency was swept through dozens of consecutive cavity longitudinal modes at a sweep rate of 5 Hz by changing the laser driving current.

In optical feedback, especially with a linear cavity, the stringent constraint on feedback phase is indispensable. We leverage the symmetry of the derivative of the cavity transmission mode as an error signal and feed the correction signal to the PZT via a low frequency loop to actively regulate the length of the light propagation path as well as the feedback phase [10].

4. Results

To test the theoretical model for OF-LCEAS over a broad laser tuning range, we monitored the coupled laser frequency both on- and off-resonance using a wavemeter. In order to measure the laser frequency with high precision, the integration time of the wavemeter was set to 100 ms and the laser frequency was scanned slowly over the ~800 MHz range plotted in Fig. 4 for a long total scan time of 50 s. The measured cavity transmission is shown in Fig. 4(a), and transmission from two consecutive longitudinal modes of the linear cavity were observed. Figure 4(b) is the measured laser frequency. Clear discontinuities in the measured laser frequency are attributed to optical feedback.

By comparison with the simulated result from a slightly modified Eq. (5), plotted in Fig. 4(c), we divide the frequency behavior into three phases. In phase (1), the laser frequency (red dashed arrows) is stabilized to one cavity longitudinal mode by the cavity leak-out. Following by eye the red dashed arrow in Fig. 4(c) to the end of the stabilized region in phase (1), a turning point is reached, and the laser frequency jumps into phase (2) at which point the laser frequency is

Optics EXPRESS

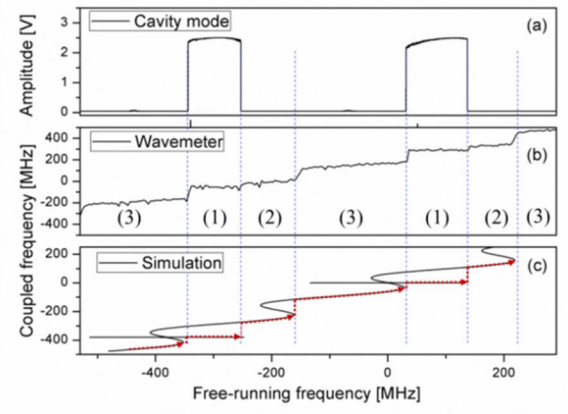

Fig. 4. Measured cavity transmission (a), showing two transmission by two longitudinal modes of the linear cavity. Comparison of measured (b) and simulated (c) laser frequency with optical feedback. Experimental set-up with $L_a \approx 2L_c$.

controlled by optical feedback from non-resonant light and is tuned almost linearly. Eventually, another turning point is reached and the laser will jump into phase (3), or the second period of the simulation where the non-resonant light dictates the coupled laser frequency. After phase (3), the coupled laser frequency will return to phase (1) and is stabilized to a second cavity mode.

In summary, the measured laser frequency in Fig. 4(b) is in good agreement with the simulation in Fig. 4(c). Note that in order to improve agreement between the model and the experiment, we empirically varied independent values of β for each of the reflected fields: non-resonant $\beta = 2\times10^{-5}$ and resonant $\beta = 13\times10^{-5}$. The physical reasoning for this choice may be traced to one of the possible perturbations to the general model mentioned at the end of the Theory section. At an approximate ratio of 1:6, the empirically adjusted β values are in good agreement with one another, suggesting that a perturbation like birefringence or preferential clipping losses in a highly mode-matched laser-cavity system is relatively small.

Figure 5(a) shows the cavity transmission without molecular absorption obtained by quickly sweeping the laser current. There are 65 successive cavity modes, verifying system reproducibility, and the total laser frequency coverage is 24 GHz. With active control of feedback phase, each mode is broadened by optical feedback and observed to be relatively symmetric and flat at their center. The mode width, i.e. the capture range, is determined by the feedback ratio, i.e. β, and is wider than hundreds of MHz when β is larger than 10^{-5}. The peak values of the mode transmission intensities, connected by a red line, decreases linearly as the laser current is decreased. Figure 5(b) shows transmission by the same series of cavity modes, but this time with intracavity absorption. The cavity was filled with ambient air at 705 Torr, and the laser frequency was tuned to address three overlapping methane transitions at around 6046.96 cm^{-1} with HITRAN linestrengths on the order of 10^{-21} cm^{-1}/(molecule cm^{-2}) [26]. The decrease in mode amplitude due to molecular absorption is clearly seen. The attenuation depends upon the gas absorption as

$$\frac{\Delta I(\nu)}{I_0(\nu)} = \frac{I_0(\nu) - I_{\text{trans}}(\nu)}{I_0(\nu)} = 1 - \frac{(1 - r_m^2)^2 \ \exp(-2\alpha_g(\nu)L_c)}{[1 - r_m^2 \ \exp(-2\alpha_g(\nu)L_c)]^2}, \tag{6}$$

where I_0 and I_{trans} are the cavity transmission intensities without and with absorption, respectively. The quantity ΔI is the transmission intensity attenuation, α_g is the absorption coefficient, and ν is the coupled laser frequency.

Optics EXPRESS

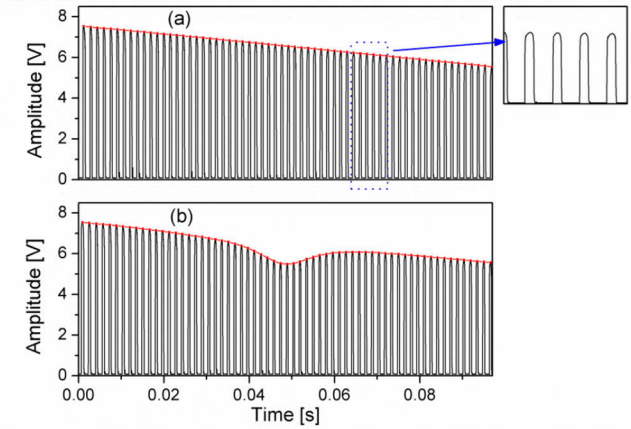

Fig. 5. The consecutive cavity modes without (a) and with (b) molecular absorption from methane, CH_4, in ambient air. The upper right panel is a zoom-in of the cavity transmission in (a) near resonance.

The values of $\Delta I/I_0$ calculated from Eq. (6) from the data in Fig. 5 are plotted in Fig. 6 as black dots. Also shown in Fig. 6 and plotted as a red line is the fitted result from a Lorentzian line shape model simulated with spectral parameters from the HITRAN database [26]. The absorption from water with strength of more than 3 orders lower than that of methane is also considered in the fitting model. The fitted residuals, shown as a black line in the lower panel, suggests good consistency between the data and the model. The retrieved CH_4 concentration is 5.16 ppm and the signal to noise ratio is 130.

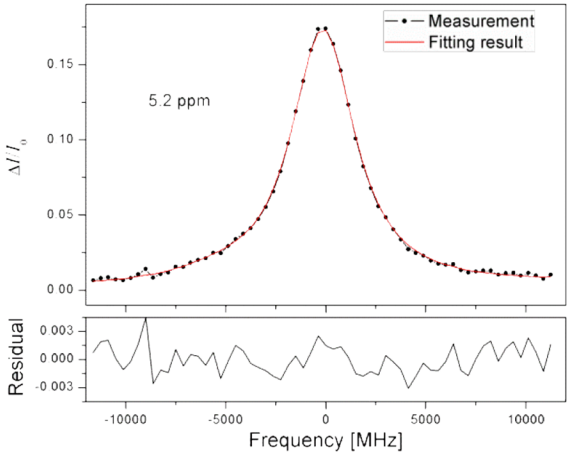

Fig. 6. Absorption spectrum of CH_4 in ambient air at 705 Torr (black dots), and the Lorentzian fitting result (red line); the fitted residuals (lower panel, black line). The measurement time is 0.1 s.

In order to evaluate the long-term stability of the system, we consecutively measured spectra from a static charge of CH_4 gas for more than 0.5 h. The black line in Fig. 7(a) is the retrieved concentration for that static gas sample, which varied about a mean value of 5.16 ppm. The noise in the retrieved concentration of CH_4 is speculated to be caused by slow shifts of the beam location on the cavity mirror which change slightly the baseline transmission level. The Allan-Werle plot

Optics EXPRESS

[27] is shown in Fig. 7(b). The white response of the system is 4.1×10^{-9} cm^{-1} Hz$^{-1/2}$. Taking into account the low finesse of the current cavity, this result is comparable to the performance of CRDS systems. We suspect this is partly because the optical feedback, accompanied by balanced detection, can largely eliminate laser intensity noise as well as variations in the laser coupling efficiency. The detection limit is obtained at 30 s with 1.3×10^{-9} cm^{-1}, corresponding to a minimal detection CH_4 concentration of 3.1 ppb.

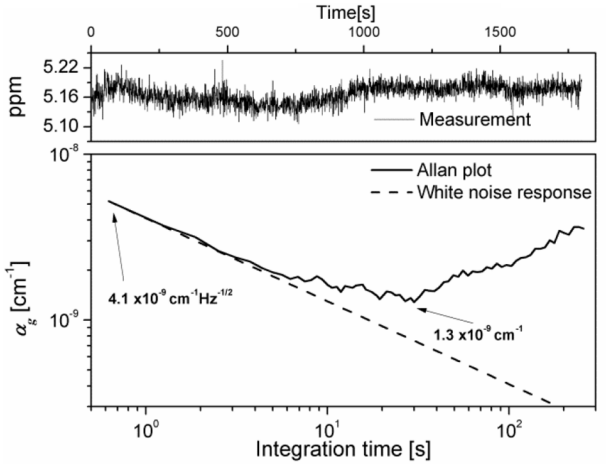

Fig. 7. (a) Retrieved concentrations from a long-term monitor of a set of CH_4 gas (b) Allan-Werle variance plot.

Finally, we exploited the OF-LCEAS system to monitor CH_4 concentration in the air outside of our laboratory located in Taiyuan, China. A gas pump was utilized to extract the air and, after a dehumidifier and micronic filter, continuously fill the cavity with new sample. Figure 8 shows the concentration results recorded over 3 consecutive days spanning from January 10, 2021 at 14:30 to January 13, 2021 at 14:30 local time. The variation of CH_4 concentration in the sampled anthropic zone depends on both human activity and local weather. The low and stable

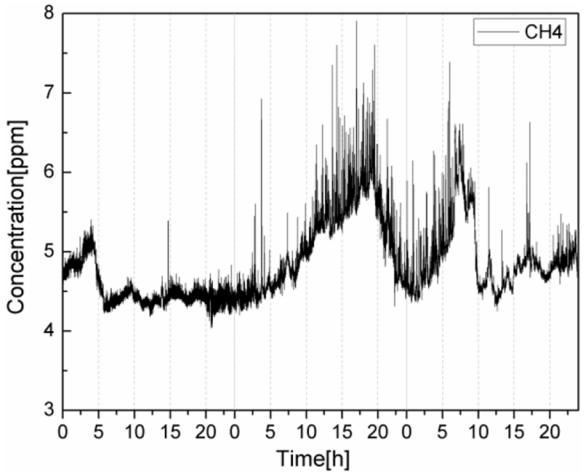

Fig. 8. Monitoring of CH_4 concentration in a sampling of the local atmosphere for 3 days.

Optics EXPRESS

levels observed during the first day and end of the third day are suspected to be because of severe weather with strong winds and a lack of human activity outside.

5. Conclusion

In summary, we have developed optical feedback linear cavity enhanced spectroscopy (OF-LCEAS). The theoretical analysis indicates that only the leak-out light from the cavity can give rise to optical feedback at the cavity resonance frequency if the feedback phase is properly controlled. Therefore, the laser could be tightly stabilized to successive cavity longitudinal modes without the need for high-bandwidth electronic feedback loops. By current tuning of a near-infrared distributed feedback diode laser, 65 consecutive and broadened cavity modes of a Fabry-Pérot cavity with modest finesse of 3900 were observed in transmission. With the aid of balanced detection, the detection sensitivity of 1.3×10^{-9} cm^{-1} was been achieved in 30 s of averaging. This novel methodology demonstrates the potential universality of CEAS using linear cavities and could be a powerful and transformative tool for trace gas detection.

Funding. National Key Research and Development Program of China (2017YFA0304203); National Natural Science Foundation of China (61875107, 61905134, 61905136); 111 Project (D18001); National Institute of Standards and Technology.

Acknowledgements. We thank Erin M. Adkins and Griffin J. Mead (NIST) for commenting on the manuscript.

Disclosures. The authors declare no conflicts of interest.

Data availability. Data underlying the results presented in this paper are not publicly available at this time but may be obtained from the authors upon reasonable request.

References

1. "Introduction to Cavity Enhanced Absorption Spectroscopy," in *Cavity-enhanced spectroscopy and Sensing*, G. Gagliardi and L. Hans-Peter, eds. (Springer, 2014).
2. B. A. Paldus and A. A. Kachanov, "An historical overview of cavity-enhanced methods," Can. J. Phys. **83**(10), 975–999 (2005).
3. G. D. Cole, W. Zhang, B. J. Bjork, D. Follman, P. Heu, C. Deutsch, L. Sonderhouse, J. Robinson, C. Franz, A. Alexandrovski, M. Notcutt, O. H. Heckl, J. Ye, and M. Aspelmeyer, "High-performance near- and midinfrared crystalline coatings," Optica **3**(6), 647–656 (2016).
4. L. Pinard, B. Sassolas, R. Flaminio, D. Forest, A. Lacoudre, C. Michel, J. L. Montorio, and N. Morgado, "Toward a new generation of low-loss mirrors for the advanced gravitational waves interferometers," Opt. Lett. **36**(8), 1407–1409 (2011).
5. M. Zaborowski, M. Slowinski, K. Stankiewicz, F. Thibault, A. Cygan, H. Jozwiak, G. Kowzan, P. Maslowski, A. Nishiyama, N. Stolarczyk, S. Wojtewicz, R. Ciurylo, D. Lisak, and P. Wcislo, "Ultrahigh finesse cavity-enhanced spectroscopy for accurate tests of quantum electrodynamics for molecules," Opt. Lett. **45**(7), 1603–1606 (2020).
6. J. Morville, D. Romanini, M. Chenevier, and A. Kachanov, "Effects of laser phase noise on the injection of a high-finesse cavity," Appl. Opt. **41**(33), 6980–6990 (2002).
7. J. J. Scherer, J. B. Paul, A. Okeefe, and R. J. Saykally, "Cavity ringdown laser absorption spectroscopy: History, development, and application to pulsed molecular beams," Chem. Rev. **97**(1), 25–52 (1997).
8. D. S. Baer, J. B. Paul, J. B. Gupta, and A. O'Keefe, "Sensitive absorption measurements in the near-infrared region using off-axis integrated-cavity-output spectroscopy," Appl. Phys. B: Lasers Opt. **75**(2-3), 261–265 (2002).
9. D. Romanini, M. Chenevier, S. Kassi, M. Schmidt, C. Valant, M. Ramonet, J. Lopez, and H. J. Jost, "Optical-feedback cavity-enhanced absorption: a compact spectrometer for real-time measurement of atmospheric methane," Appl. Phys. B **83**(4), 659–667 (2006).
10. D. J. Hamilton and A. J. Orr-Ewing, "A quantum cascade laser-based optical feedback cavity-enhanced absorption spectrometer for the simultaneous measurement of CH4 and N2O in air," Appl. Phys. B **102**(4), 879–890 (2011).
11. E. R. T. Kerstel, R. Q. Iannone, M. Chenevier, S. Kassi, H. J. Jost, and D. Romanini, "A water isotope (H-2, O-17, and O-18) spectrometer based on optical feedback cavity-enhanced absorption for in situ airborne applications," Appl. Phys. B **85**(2-3), 397–406 (2006).
12. P. Cermak, M. Triki, A. Garnache, L. Cerutti, and D. Romanini, "Optical-Feedback Cavity-Enhanced Absorption Spectroscopy Using a Short-Cavity Vertical-External-Cavity Surface-Emitting Laser," IEEE Photonics Technol. Lett. **22**(21), 1607–1609 (2010).
13. I. Courtillot, J. Morville, V. Motto-Ros, and D. Romanini, "Sub-ppb NO2 detection by optical feedback cavity-enhanced absorption spectroscopy with a blue diode laser," Appl. Phys. B **85**(2-3), 407–412 (2006).

Optics EXPRESS

14. J. Morville, S. Kassi, M. Chenevier, and D. Romanini, "Fast, low-noise, mode-by-mode, cavity-enhanced absorption spectroscopy by diode-laser self-locking," Appl. Phys. B **80**(8), 1027–1038 (2005).
15. A. G. V. Bergin, G. Hancock, G. A. D. Ritchie, and D. Weidmann, "Linear cavity optical-feedback cavity-enhanced absorption spectroscopy with a quantum cascade laser," Opt. Lett. **38**(14), 2475–2477 (2013).
16. Y. Zhao, S. Wang, Z. Fang, T. Li, and E. Zang, "High-finesse F-P Cavity External Optical Feedback Narrow Linewidth Diode Laser," in *2013 International Conference on Optical Instruments and Technology: Optoelectronic Devices and Optical Signal Processing*, Y. Dong, X. Bao, C. Lu, and X. Xin, eds. (2013).
17. M. Durand, J. Morville, and D. Romanini, "Shot-noise-limited measurement of sub-parts-per-trillion birefringence phase shift in a high-finesse cavity," Phys. Rev. A **82**(3), 031803 (2010).
18. G. Zhao, D. M. Bailey, A. J. Fleisher, J. T. Hodges, and K. K. Lehmann, "Doppler-free two-photon cavity ring-down spectroscopy of a nitrous oxide (N2O) vibrational overtone transition," Phys. Rev. A **101**(6), 062509 (2020).
19. G. Zhao, J. Tian, J. T. Hodges, and A. J. Fleisher, "Frequency stabilization of a quantum cascade laser by resonant feedback from a linear two-mirror cavity," Opt. Lett. **46**(13), 3057–3060 (2021).
20. P. Laurent, A. Clairon, and C. Breant, "Frequency noise analysis of optically self-locked diode lasers," IEEE J. Quantum Electron. **25**(6), 1131–1142 (1989).
21. A. E. Siegman, *Lasers* (University Science Books, 1986).
22. K. M. Manfred, L. Ciaffoni, and G. A. D. Ritchie, "Optical-feedback cavity-enhanced absorption spectroscopy in a linear cavity: model and experiments," Appl. Phys. B **120**(2), 329–339 (2015).
23. Certain commercial equipment is identified in this paper in order to specify the experimental procedure adequately. Such identification is not intended to imply recommendation or endorsement by the National Institute of Standards and Technology (NIST), nor is it intended to imply that the equipment identified is necessarily the best available for the purpose.
24. G. Zhao, T. Hausmaninger, W. Ma, and O. Axner, "Differential noise-immune cavity-enhanced optical heterodyne molecular spectroscopy for improvement of the detection sensitivity by reduction of drifts from background signals," Opt. Express **25**(23), 29454–29471 (2017).
25. C. J. Hood, H. J. Kimble, and J. Ye, "Characterization of high-finesse mirrors: Loss, phase shifts, and mode structure in an optical cavity," Phys. Rev. A **64**(3), 033804 (2001).
26. I. E. Gordon, L. S. Rothman, C. Hill, R. V. Kochanov, Y. Tan, P. F. Bernath, M. Birk, V. Boudon, A. Campargue, K. V. Chance, B. J. Drouin, J. M. Flaud, R. R. Gamache, J. T. Hodges, D. Jacquemart, V. I. Perevalov, A. Perrin, K. P. Shine, M. A. H. Smith, J. Tennyson, G. C. Toon, H. Tran, V. G. Tyuterev, A. Barbe, A. G. Csaszar, V. M. Devi, T. Furtenbacher, J. J. Harrison, J. M. Hartmann, A. Jolly, T. J. Johnson, T. Karman, I. Kleiner, A. A. Kyuberis, J. Loos, O. M. Lyulin, S. T. Massie, S. N. Mikhailenko, N. Moazzen-Ahmadi, H. S. P. Mueller, O. V. Naumenko, A. V. Nikitin, O. L. Polyansky, M. Rey, M. Rotger, S. W. Sharpe, K. Sung, E. Starikova, S. A. Tashkun, J. Vander Auwera, G. Wagner, J. Wilzewski, P. Wcislo, S. Yu, and E. J. Zak, "The HITRAN2016 molecular spectroscopic database," J. Quant. Spectrosc. Radiat. Transfer **203**, 3–69 (2017).
27. P. Werle, R. Mucke, and F. Slemr, "The limits of signal averaging in atmospheric trace-gas monitroing by tunable diode-laser absorption-spectroscopy(TDLAS)," Appl. Phys. B **57**(2), 131–139 (1993).